PERGAMON

Computerized Medical Imaging and Graphics 25 (2001) 277–286

Computerized Medical Imaging and Graphics

www.elsevier.com/locate/compmedimag

Myocardium extraction in positron emission tomography based on soft computing

F. Behloul[a], A. Boudraa[b], B.P.F. Lelieveldt[a], M. Janier[c], J.H.C Reiber[a,*]

[a]*Division of Image Processing (LKEB), Department of Radiology, Leiden University Medical Center, P.O. Box 9600, 2300 RC Leiden, Netherlands*
[b]*L2TI Institut Galilée, Université Paris 13, Avenue J.B. Clément, 93430 Villetaneuse, France*
[c]*Research and Applications Center for Image and Signal Processing (CREATIS), 59 Bd Pinel 69003 Lyon, France*

Received 19 May 2000; accepted 17 July 2000

Abstract

This paper presents an efficient and accurate approach to myocardium extraction in Positron Emission Tomography (PET) images based on a careful application of soft computing techniques. PET images present a noisy background, making the automatic myocardium extraction and uptake quantification a difficult task. In this work a Self Organized Radial Basis Function Network (SRBFN) is designed to focus on the myocardium in an iterative process until the total extraction of the myocardium from the noisy background is achieved. Fuzzy sets and fuzziness measures are used to compute the error of the network. The method was tested on a set of nine images of different patients and its effectiveness is illustrated in two patients showing tracer uptake defects.

Keywords: Object extraction; Positron emission tomography; Soft computing; Radial basis function network; Fuzziness measures

1. Introduction

Positron Emission Tomography (PET) has enhanced the understanding of the biochemistry of normal and abnormal functions within the body. PET provides the means for imaging the rates of biological processes in vivo. Since the location and the extent of the disease are unknown in most cases, the primary objective of this work was to develop an efficient means of searching throughout the three-dimensional (3D) image to determine the disease location. Recognition depends upon the type of information both in terms of interpreting what it means and how sensitive it is to identify the presence of a disease.

Analysis of PET heart images may be performed by simple visual evaluation slice by slice. This operation is tedious and suffers from observer bias. As an alternative to this visual evaluation, information can be represented using a polar-map technique. A polar map is derived from multiple planes so that information about the entire myocardium can be displayed in a single image. This map can be thought of as the image that would be obtained if one looks at the Left Ventricle (LV) as a 3D cone shaped object and projected onto a single plane (Fig. 1). This form of display has the advantage that all areas of myocardium are represented in a single image, but it is less easy to assess the relationship between the defected region and coronary arterial territories [1]. Both approaches (slice by slice visualization and polar maps) do not allow an easy assessment of the extent of the tracer uptake defect on the LV. Thus, a 3D visualization approach presenting accurate localization and extent of the disease is desirable.

Since PET images of the heart present a noisy background, image segmentation or object extraction is required for a good visualization and interpretation. To tackle real-world image-segmentation problems, it is frequently advantageous to use several computing techniques synergically rather than exclusively. This results in the construction of hybrid systems that combine knowledge, techniques and methodologies from various sources. A successful combination is that of neural network approaches and fuzzy set theory, which is referred to as a neuro-fuzzy model. The neural network has the ability to adapt itself via learning procedures while fuzzy set theory provides a systematic calculus to deal with imprecise and incomplete information. The integration of these two complementary approaches, together with certain derivative-free optimization techniques such as genetic algorithms, results in a new discipline called Soft Computing.

In this paper, we present an original and successful neuro-fuzzy approach to extract compact objects in noisy images.

* Corresponding author. Tel.: +31-71-526-3935/2138; fax: +31-71-526-6801.
E-mail address: reiber@lkeb.azl.nl (J.H.C. Reiber).

0895-6111/01/$ - see front matter
PII: S0895-6111(00)00067-7

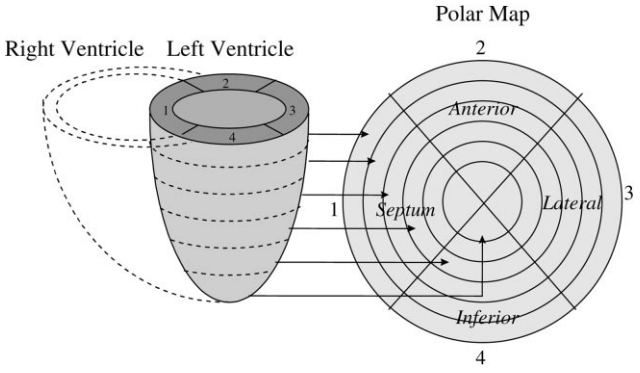

Fig. 1. Polar map 3D image representation. The inner circle represents the apex whereas the outer circle represents the basal part of the LV.

A Radial Basis Function Network (RBFN) is used to extract compact regions through a self-organization process using only one noise corrupted image. The error of the RBFN is computed using concepts of fuzzy sets and fuzziness measures [2]. Our approach is derived from that of Gosh et al. [2].

The paper is organized as follows. In the next section we will provide a brief description of PET images as used in this work and show the difficulty of their 3D visualization using a simple approach (thresholding and ray tracing). In Sections 3 and 4 the basic definition of RBFNs and fuzziness measures, respectively, will be recalled. The synergistic use of both models (Self Organized Radial Basis Function Network (SRBFN)) for object extraction is presented in Section 5. Section 6 shows the performances of the SRBFN applied to PET images, and Section 7 discusses these results. Concluding remarks are given in Section 8.

2. ^{18}FDG PET images of the heart

PET imaging is accomplished through the integration of two technologies: the tracer kinetic assay method and Computed Tomography (CT). The tracer assay method uses a radiolabeled biologically active compound (tracer) and a mathematical model that describes the kinetics of the tracer as it participates in a biological process. The PET scanner provides measurement of the tissue tracer concentration required by the tracer kinetic model. [F-18] Fluoro-2-deoxy-glucose (^{18}FDG), an F-18-labeled analog of glucose, is used in PET to study glucose metabolism. After a bolus injection into the blood, ^{18}FDG enters the tissue and is phosphorylated into FDG-6-phosphate (FDG-6-P). During a ^{18}FDG PET study, the endogenous glucose level is relatively constant (i.e. at a steady state). Using a gray scale, black indicates lowest concentration and white indicates highest concentration. A three-dimensional (3D) image of the anatomic distribution of the biological process under study is reconstructed. Slices of the obtained volume in short axis view (orthogonal to the principal axis of the heart) are presented in Fig. 2. At the beginning of an ^{18}FDG PET study, ^{18}FDG is absent in both blood and tissue. Following a bolus injection, ^{18}FDG initially peaks in the blood and then accumulates in the tissue. Cardiac ^{18}FDG PET images are generally involved in viable myocardium assessment studies.

The quantification of the viable tissue for a patient having coronary artery disease can help to decide whether or not the patient will benefit from a revascularisation procedure. In general, three levels of ^{18}FDG uptake are distinguished by the clinicians: low, intermediate and high. Normal or remote myocardium is expected to have a high uptake level exceeding 70% of the maximal value in the image (assuming that the maximum value corresponds to a normal tissue). Seriously damaged or infarcted tissues have a low uptake rate (less than 50%). However, it is very difficult to diagnose the ischemic processes involved in the studied dysfunctional myocardium based only on PET 18-FDG images and especially when 18-FDG uptake is intermediate (50–70%). A medium (intermediate) uptake region may correspond to a partially infarcted tissue (heterogeneous) or a homogeneously reduced metabolic function. Because of the doubt, some clinicians rather classify these regions into the viable category.

Ideally, a threshold value in the range of 50–60% of the max value should allow the visualization of viable myocardium. However, due to the noisy nature of PET images, a simple thresholding technique, generally provided in the software of the scanner console, does not seem to be suitable for a 3D extraction and visualization of the viable myocardium (Fig. 3). Indeed, in some images, some pathological regions are not visible (Fig. 3a) and thus a higher threshold value is needed. However, an increased threshold value tends to overestimate the extent of already detected defects

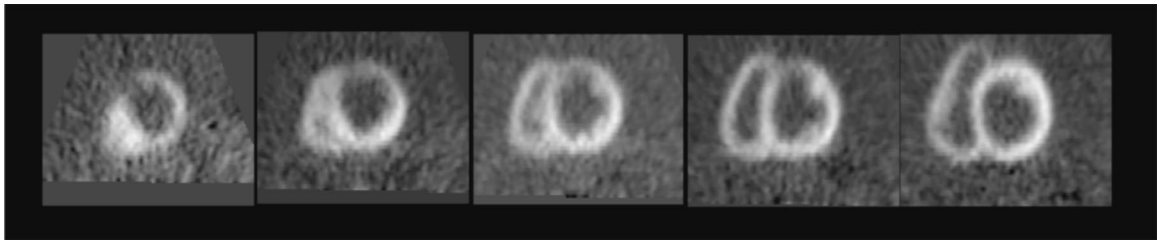

Fig. 2. ^{18}FDG Short axis slices from apex (on the left) to base (on the right).

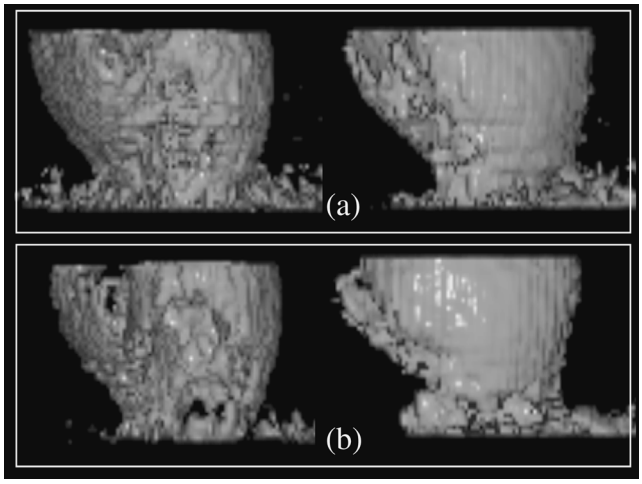

Fig. 3. Volume visualization in two orthogonal views after a simple thresholding: (a) threshold = 50%; (b) threshold = 75%.

and to thin down the myocardium (Fig. 3b). There is obviously a need for more sophisticated methods to accurately distinguish viable myocardium from the background.

3. Radial basis function networks

Radial Basis Functions (RBFs) are primarily used to solve interpolation problems (fitting a curve exactly through a set of points) [3–5] and, more recently, extended to perform the more general task of approximation [6–8]. In particular, Poggio and Girosi [8] show how RBFs can be derived from classical regularization for handling ill-posed problems.

The RBFN is a feedforward neural network, which accomplishes a non-linear input–output mapping by linear combination of non-linearly transformed inputs according to the following:

$$o_j = \sum_{i=1}^{m} w_i \phi_i(x) \tag{1}$$

where x is the input vector, o_j the output of the jth output node and w_i are the output linear combining weights. The $\phi_i(x)$ are RBFs and m is the number of RBFs. Fig. 4 shows the network representation with RBF kernels represented as neurons of the hidden layer. An output of the network is a simple linear combination of the hidden neuron outputs.

RBFNs may differ in type of RBFs used and in training method. Consequently, the different types of RBFNs differ in performance. The most distinguishing feature of RBFs is that they are local, i.e. they give a significant response only in a neighborhood near a central point. Their response decreases monotonically with distance from a central point. Strictly speaking, functions whose response increases monotonically away from a central point are also RBFs, but because they are not local, they are less interesting for classification applications. RBF parameters are its center, its shape, and its width.

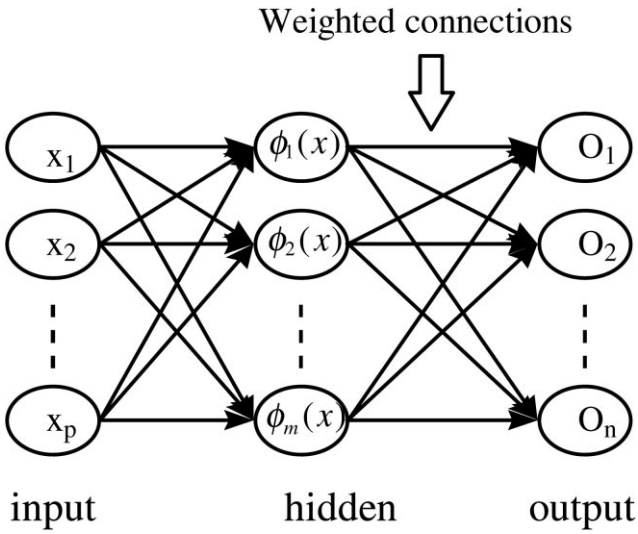

Fig. 4. RBFN with n output nodes. Each component of the input vector x feeds forward to m RBF nodes whose outputs are linearly combined with weights $\{w_{ij}, i = 1,\ldots n, j = 1\ldots m\}$ into the network output nodes.

A typical local RBF is the Gaussian function. Centered at c and of width (or radius) r, it has the form:

$$G(x, c, r) = \exp\left(\frac{\|x - c\|_R^2}{2r^2}\right) \text{ where } \|x - c\|_R^2$$

$$= (x - c)^{\mathrm{T}} R^{-1} (x - c) \tag{2}$$

where R is a positive definite matrix. Usually, the identity matrix is used.

Other common choices of radial functions are the multiquadric function:

$$\mathrm{mq}(x, c, r) = \sqrt{\|x - c\|_R^2 + r^2} \tag{3}$$

the thin-plate-spline function

$$\mathrm{tps}(x, c) = \|x - c\|_R^2 \log(\|x - c\|_R) \tag{4}$$

and the inverse multiquadric function

$$\mathrm{Imq}(x, c, r) = \frac{1}{\sqrt{\|x - c\|_R^2 + r^2}} \tag{5}$$

Gaussian-like functions (local) are more commonly used than multiquadric-like functions (non-local) which have a global response. Since Broomhead and Lowe's 1988 seminal paper [6], RBFNs have traditionally been associated with radial functions in a single hidden layer. The hidden and the output layers are generally trained sequentially: the radial function parameters are first fixed and the optimal linear combining weights are then computed [9,10]. Once the number of nodes and the parameters of the RBFs are defined, the hidden layer performs a fixed non-linear transformation; it maps the input space into a new space. The output layer then implements a linear combiner on this new space. The only output layer parameters to adjust are the

weights of this linear combiner. In general, the output weights of a RBFN can be determined by a pseudo-inverse matrix. When applied to supervised learning with linear models, the Least Square (LS) principle leads to a particularly simple optimization problem [11]. However, this approach can be computationally demanding when the training set is large. In this case, delta-rule type of learning algorithm is preferred since it is a less demanding technique.

In this work, the backpropagation (BP) algorithm is used to train the output layer. The procedure for learning the correct set of weights is to vary the weights in a manner such that the error (E) is reduced. In supervised training, a set of input–output pairs is supplied. The error of the network is generally computed by

$$E = \frac{1}{2}\sum_{j=1}^{N}(t_j - o_j)^2 \tag{6}$$

where o_j is the spontaneous output of node j and t_j is the expected output of node j N is the total number of output units. However, in our application we do not have a target image for each patient. The network is supposed to extract the heart from the noisy image based only on the contrast between myocardium and background. As the human eye would do, the network will have to focus on the object in the noisy image until it becomes 'clear'. Thus, a measure of fuzziness of the image can be considered as the error of the network, to be reduced. In this work, two fuzziness measures have been considered (index of fuzziness and fuzzy entropy). In order to facilitate their presentation, a brief introduction to fuzzy sets and fuzziness measures is given in the following section.

4. Fuzzy sets and fuzziness measures

A fuzzy set F is characterized by a membership function $\mu_F(x)$ that associates to each point x in a space of points X a real number in the interval [0,1]. The value $\mu_F(x)$ represents the grade of membership of x in F. $\mu_F(x) = 1$ indicates a strict containment of x in F and $\mu_F(x) = 0$ means that x does not belong to F. Any intermediate value would indicate the degree to which x is an element of F. Formally, a fuzzy set F that has a finite number of elements $x_1, x_2, \ldots, x_n$ is defined as a collection of pairs

$$F = \{(\mu_F(x_i), x_i), i = 1, 2, \ldots, n\}$$

A measure of fuzziness estimates the average ambiguity in a fuzzy set. Intuitively, the fuzziness of a crisp set using any measure should be zero (or minimum), as there is no ambiguity about whether an element belongs to the set or not. If the set is maximally ambiguous then the fuzziness measure should be maximal. When the membership value approaches either to 0 or 1, the ambiguity of the set decreases. Thus, a fuzzy set is most ambiguous when $\mu_F(x) = 0.5\ \forall x$.

The degree of fuzziness ($I(F)$) of a fuzzy set represents the amount of ambiguity in making the decision whether a point belongs to the set or not. Such a measure should have the following properties:

(i) $I(F) =$ minimum *iff* $\mu_F(x_i) = 0$ or 1 $\forall$i.
(ii) $I(F) =$ minimum *iff* $\mu_F(x_i) = 0.5\ \forall$i.
(iii) $I(F) \geq I(F^*)$, where F^* is a sharpened version of F given by

$$\mu_{F^*}(x_i) \geq \mu_F(x_i) \quad \text{if} \quad \mu_F(x_i) \geq 0.5$$

$$\leq \mu_F(x_i) \quad \text{if} \quad \mu_F(x_i) \leq 0.5$$

(iv) $I(F) = I(F^c)$, where F^c is the complement of F.

Such measures have been proposed by several authors [12–16]. Two mathematical models of fuzziness measures are used: the index of fuzziness and the fuzzy entropy. The measures considered here have been used in Ref. [2]. Both measures presented below lie in the interval [0,1] and satisfy the properties (i)–(iv).

4.1. Index of fuzziness

Let F be a fuzzy set, the index of fuzziness of F is defined by

$$v(F) = \frac{2}{n^k} d(F, \underline{F}), \tag{7}$$

where $\underline{F}$ is the nearest ordinary set to F given by

$$\mu_{\underline{F}}(x) = \begin{cases} 0 & \text{if} \quad \mu_F(x) \leq 0.5 \\ 1 & \text{if} \quad \mu_F(x) \geq 0.5 \end{cases} \tag{8}$$

$d(F, \underline{F})$ is the distance between the two sets F and $\underline{F}$. The value of k depends on the type of the distance used. $k = 1$ corresponds to the generalized Hamming distance and $k = 0.5$ to the Euclidean distance. The corresponding index of fuzziness is called the quadratic index of fuzziness $v_q(F)$.

$$v_q(F) = \frac{2}{\sqrt{n}} \sum_{i=1}^{n} \sqrt{(\mu_F(x_i) - \mu_{\underline{F}}(x_i))^2} \tag{9}$$

The index of fuzziness reflects the ambiguity of a fuzzy set by measuring the distance between its fuzzy property plane and the nearest ordinary plane.

4.2. Fuzzy entropy

Pal and Pal proposed an exponential entropy [14] given by

$$H(F) = \frac{1}{n(\sqrt{e} - 1)} \sum_{i=1}^{n} (S_n(\mu_F(x_i)) - 1)$$

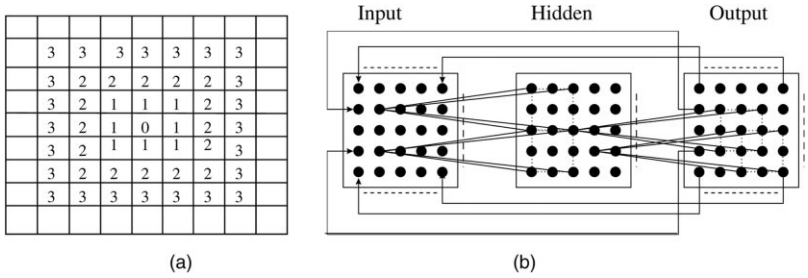

Fig. 5. Self organized RBFN. (a) neighborhood system. Pixel marked 1 belongs to the neighborhood N^1. Those marked 2 belong to N^2 and so on. $N^1 \subset N^2 \subset N^3$. (b) RBFN topology.

with

$$S_n(\mu_F(x_i)) = \mu_F(x_i)\, e^{1-\mu_F(x_i)} + (1 - \mu_F(x_i))\, e^{\mu_F(x_i)} \quad (10)$$

The meaning of the term 'entropy' is quite different from the one of classical entropy because no probabilistic concept is needed to define it. The function $H(F)$ gives a measure of the average amount of difficulty in taking a decision on any element of the fuzzy set.

A gray value image can be considered as a fuzzy set 'Bright'. By re-scaling the dynamics of the image from [0,…,255] to [0,…,1] a membership degree to the fuzzy set bright is derived for each pixel.

When applied on an image, both fuzziness measures (index and entropy) give an idea of 'indefiniteness' of the image. They may be considered as measures of average intrinsic information that is received when one has to make a decision in order to classify the pixels described by a fuzzy set. In the following section we show how the two fuzziness measures are used to compute the error of a RBFN making the network self-organized.

5. Self-organized radial basis function network

5.1. The network characteristics

The architecture of the proposed SRBFN consists of three layers: the input layer, one hidden (RBF) layer and the output layer. In every layer, there are $X \times Y$ neurons (for an $X \times Y$ image): each neuron corresponds to a single pixel. Neurons in the same layer are not connected to each other. Each neuron is connected to the corresponding neuron and its neighbors in the next layer (Fig. 5). The neighborhood considered in this work is shown in Fig. 5a. Pixel labeled '1' belongs to the neighborhood N^1. Those marked 2 belong to N^2 and so on. $N^1 \subset N^2 \subset N^3$…. In other words, N^1 corresponds to the eight $(3 \times 3 - 1)$ nearest neighbors (N^1) or the 24 $(5 \times 5 - 1)$ nearest neighbors (N^2) and so on.

The SRBFN differs from the standard RBFN in three ways:

- The layers are partially connected and the neurons have spatial positions corresponding to the pixels in the image
- The feedback connections from the output layer to the inputs make the network recurrent. The output is considered as input for the next iteration.
- A sigmoid function f is used for the activation of the output nodes

$$o_j = f(I_j) \text{ where } I_j = \sum_{i=1}^{m} w_i \phi_i(x) \text{ and } f(x) = \frac{1}{1 + e^{-(x-\theta)}} \quad (11)$$

where θ is a bias value and $\phi_i(x)$ are Gaussian RBFs.

The output of each neuron of the hidden and output layers lies in [0,1]. It represents the degree of brightness of the corresponding pixel in the image. The measure of fuzziness of the fuzzy set Bright is viewed as the error of the network. After the weights have been adjusted according to the error measure, the neurons in the output layer are fed back to the corresponding neurons in the input layer. The output values of the output nodes, which lie in [0,1], are considered to be the brightness degrees of the corresponding pixels (0 for black, 1 for white, and any intermediate value is a gray level). The gray levels corresponding to the output values are considered as the input of the next iteration.

5.2. Training

The BP algorithm is used to train the output layer. The change in weights reducing the error E is given by

$$\Delta w_{ij} = \eta \left(- \frac{\partial E}{\partial o_j} \right) f'(I_j) o_i \quad (12)$$

where η is a learning rate. The sigmoid function is used because of its simple derivative function

$$f'(I_j) = \frac{\partial o_j}{\partial I_j} = o_j(1 - o_j) \quad (13)$$

The mathematical derivations of the BP for each fuzziness measure are given below:

A. Weight change for quadratic index of fuzziness

Let the error be:

$$E = g(v_q) = v_q^2 \text{ where } v_q^2 = \frac{4}{n} \left[\sum_j \{\min(o_j, (1 - o_j))\}^2 \right] \quad (14)$$

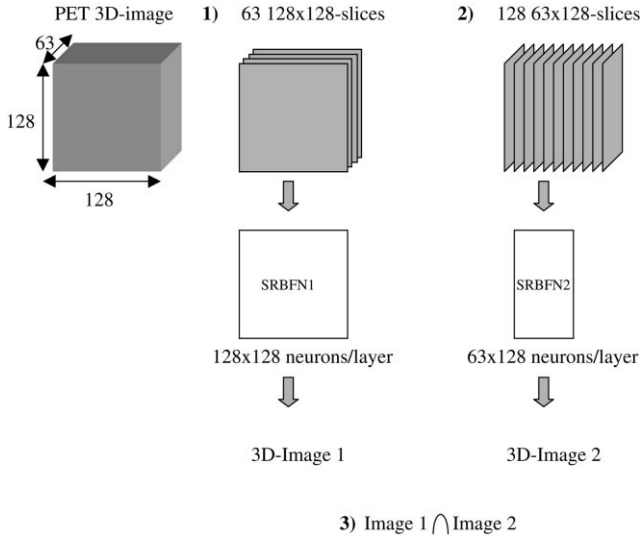

Fig. 6. Sequential processing of the 2D slices of the PET image. Two orthogonal views are considered. The interaction of the obtained images is retained as the final result of the myocardium extraction process.

where n is the number of the output units. Thus

$$-\frac{\partial E}{\partial o_j} = \begin{cases} -\frac{4}{n}(-2o_j) & \text{if } 0 \le o_j \le 0.5 \\ \frac{4}{n}(2(1-o_j)) & \text{if } 0.5 \le o_j \le 1 \end{cases} \tag{15}$$

$$\Delta w_{ij} = \begin{cases} \eta_1 \frac{4}{n}(-2o_j) f'(I_j) o_j & \text{if } 0 \le o_j \le 0.5 \\ \eta_1 \frac{4}{n}(2(1-o_j)) f'(I_j) o_j & \text{if } 0.5 \le o_j \le 1 \end{cases} \tag{16}$$

or

$$\Delta w_{ij} = \begin{cases} \eta(-o_j) f'(I_j) o_j & \text{if } 0 \le o_j \le 0.5 \\ \eta(1-o_j) f'(I_j) o_j & \text{if } 0.5 \le o_j \le 1 \end{cases} \tag{17}$$

where $\eta = \eta_1 \times (4/n) \times 2$.

B. Weight change for exponential entropy

Let the error be:

$$E = g(H) = H$$

$$H(A) = \frac{1}{n(\sqrt{e}-1)} \sum_{j=1}^{n} (o_j\, e^{1-o_j} + (1-o_j)\, e^{o_j} - 1) \tag{18}$$

$$\frac{\partial H}{\partial o_j} = \frac{1}{n(\sqrt{e}-1)} ((1-o_j)\, e^{1-o_j} - o_j\, e^{o_j}) \tag{19}$$

To make the weight correction value minimum when the membership values of the elements are 0 or 1 and maximum when they are all 0.5, we take

$$\Delta w_{ij} = -\eta_2 \frac{1}{\dfrac{\partial E}{\partial o_j}} f'(I_j) o_i \tag{20}$$

$$\Delta w_{ij} = -\eta \frac{1}{(1-o_j)\, e^{1-o_j} - o_j\, e^{o_j}} f'(I_j) o_i \tag{21}$$

where

$$\eta = \eta_2 \times n(\sqrt{e}-1)$$

$$\Delta w_{ij} = \begin{cases} -\eta \frac{1}{(1-o_j)\, e^{1-o_j} - o_j\, e^{o_j}} f'(I_j) o_i & \text{if0 } \le o_j \le 0.5 \\ \eta \frac{1}{o_j\, e^{o_j} - (1-o_j)\, e^{1-o_j}} f'(I_j) o_i & \text{if } 0.5 \le o_j \le 1 \end{cases} \tag{22}$$

At the first iteration, the input nodes receive the gray levels of the corresponding pixel. For the hidden layer, each RBF center is localized at the value of the corresponding pixel in the image. The radii of all the RBFs are set to 256/2. The total input to any node of the output layer lies in [0, *Nl*], where *Nl* is the number of links that a neuron has. The parameter θ of the sigmoids in the output nodes is set to *Nl*/2, since *Nl*/2 corresponds to the middle most value of the total input range. All initial weights (between the hidden and output layers) are set to 1.

6. Results

The SRBFN presented above is designed to extract a compact object from one noisy 2D image. It is easy to extend the architecture to process 3D images; however, the computation complexity increases dramatically. On the other hand, we have found that the result obtained when considering the 3D image as a set of 2D slices (images) and applying the SRBFN to each slice is comparable (in terms of size and shape of the extracted object) to that when considering the total 3D image. Therefore we considered the 3D PET image as a set of 2D-images.

To evaluate the procedure described above, 9 patients were examined. ^{18}FDG uptake was imaged using a HR + tomograph (Siemens Erlangen) PET scanner. ^{18}FDG (0.05 mci/kg) was injected as a slow bolus. A 3D volume (63 slices) taken 45 min after the infusion with 15 min acquisition time was acquired. Two orthogonal views were considered (Fig. 6): 63 128 × 128-slices and 128 63 × 128-slices; the intersection of the two independently extracted objects constitutes the final result of the myocardium extraction process.

Different sizes of neighborhood were tested and N^2 turned out to be the best compromise between processing time and accuracy of shape and width of the extracted myocardium.

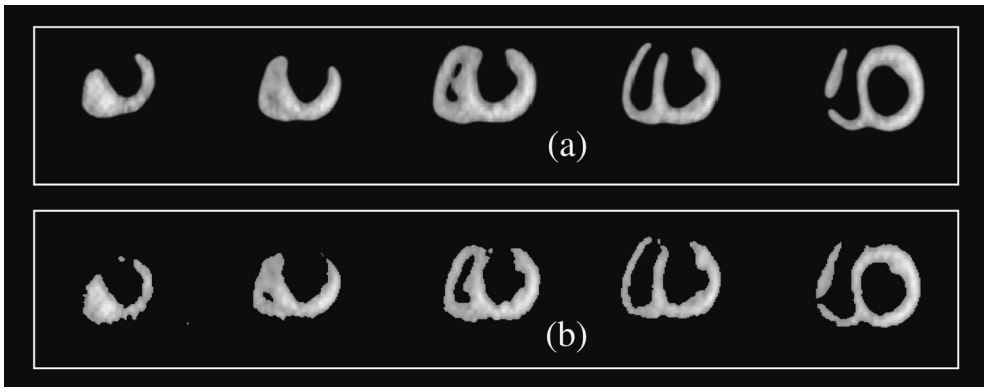

Fig. 7. Object extraction results. (a) Index of fuzziness. (b) Fuzzy entropy.

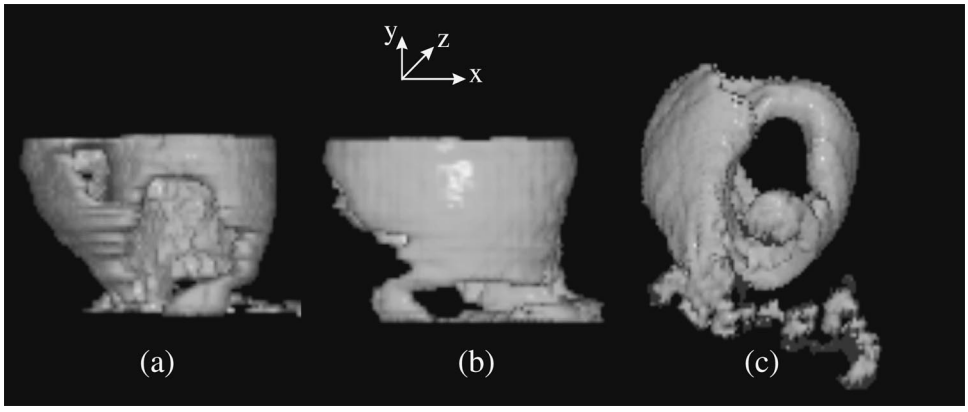

Fig. 8. Volume rendered visualization of the entropy extracted myocardium: The diseased region appears as a hole in the myocardium. (a) Orthogonal view of the heart showing a defect in almost all the posterior wall of the LV. (b) 90° *Y* rotation of (a) showing the extend of the disease in the apical anterior wall of the LV (c) 45°. *X* rotation of (a) showing both defects (posterior and apical anterior) and the right ventricle.

Fig. 7 shows the results obtained using the index of fuzziness versus those obtained using the entropy measure. The diseased area appears as a hole in the myocardium (Fig. 8). For the index of fuzziness (Fig. 7a), the diseased region and the myocardium width are overestimated (over-smoothed), while the compactness of the extracted object is nicely preserved. However, for the entropy measure (Fig. 7b), the results were very much closer to manually delineated regions but the compactness of the object was not always preserved.

Using the index of fuzziness, the network requires more time to stabilize. Indeed, the index of fuzziness required up to 100 iterations to stabilize, while for the entropy measure, the system converges after a maximum of 5 iterations.

To take advantage of the main positive features of both fuzziness measures in the same time: ‘smoothing and compactness’ for index of fuzziness, and ‘good shape estimation’ for the fuzzy entropy, we combined both measures. For the few first iterations of the self-organizing process (2–3 iterations), the index of fuzziness was used. Because of its low learning rate, this measure produced a contrast enhancement on the original images (Fig. 9a). Subsequently the entropy measure was applied ensuring a good shape extraction (see Fig. 9b).

The sequential application of the two fuzziness measures presented the best results. Indeed, when using separately the fuzziness measures, the network was not able to detect some regions of the myocardium where there is a low ^{18}FDG uptake (The human eye is still able to delineate such regions). Only the combination of both measures made the network successful in retaining these regions in the extracted myocardium (see arrows in Fig. 9b). Thus, it seems that the two error models complement each other perfectly for an accurate delineation of the myocardium in PET images. In Fig. 10, we show another PET image presenting a relatively good contrast between the noisy background and the viable myocardium. Thresholding images are compared to SRBFN myocardium extraction image. Fig. 10a shows the image obtained using a thresholding at a value of 60% (of the maximum uptake value). Note the persistent noise around the heart and the bad delineation of the uptake defect. The threshold value was then increased gradually and interactively to 70% (Fig. 10b). A better visual delineation of the uptake defect was possible. The amount of noise around the heart was considerably reduced but still persistent. This image may be considered as a good visualization of the viable myocardium. However, when we applied

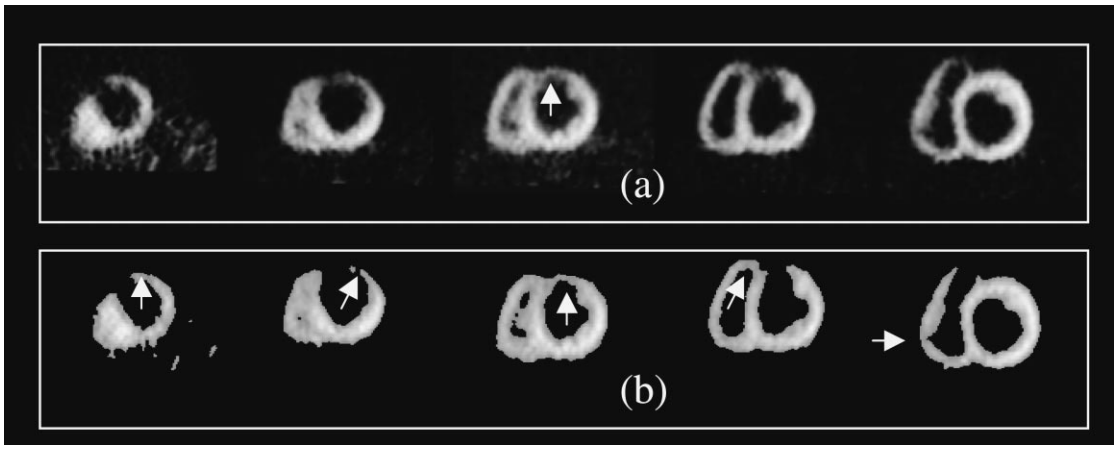

Fig. 9. Combination of both fuzzy measures. (a) Images obtained after two iterations using only the index of fuzziness measure. (b) Final result using entropy measure on the images in (a).

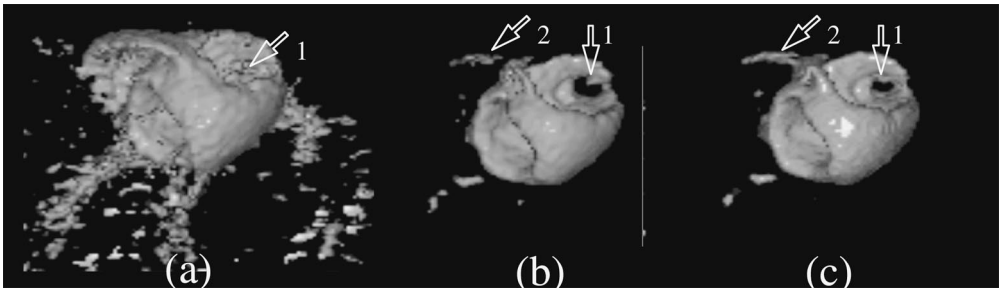

Fig. 10. Thresholding versus object extraction (a) Image obtained using as threshold value 60%. Note the persistent noise around the heart and the bad delineation of the uptake defect (arrow 1). (b) Image obtained after increasing the threshold value to 70%. Note the extent of the uptake defect especially in the apical region (arrow 1) and the disappearance of the right ventricle (arrow 2). (c) Image obtained using the SRBFN. Note the reduced amount of noise around the heart and the smaller extent of the defect (arrow 1) the anterior wall of the right ventricle is preserved (arrow 2).

the SRBFN small, but clinically highly important differences were noticed (Fig. 10c). The amount of noise was reduced even further and the apical defect seemed smaller compared to that showed in Fig. 10b (arrows 1). Arrows 2 in Fig 10b and c show the difference of compactness of the visualized object (right ventricle wall). From a clinical point of view, this does not make a difference for this patient. However, for the acknowledgment of the SRBFN tendency of compact object extraction, this is interesting to note.

The network has been tested on images from nine different patients. Based on visual comparison, the medical experts acknowledged the quality and the accuracy of the automatic viable myocardium delineation. Furthermore, the extracted image of the myocardium has been compared to Magnetic Resonance Images (MRI). This imaging modality delivers the best morphological images allowing accurate assessment of the shape and size of the heart. The LV contours drawn on the MRI image have been superimposed on the PET image of the extracted myocardium. Fig. 11 shows a representative example of the perfect correspondence between the images in terms of thickness and shape of the LV.

7. Discussion

The noisy background in PET images affects the visual interpretation of the images as well as the tracer uptake quantification. The image is considered to be ‘fuzzy’ (bad contrast between myocardium and the background). By giving a RBFN an appropriate topology (one neuron per pixel and partially connected layers) and viewing the output of the network as a fuzzy set (bright), fuzziness measures have been used to measure the error of the network, making it self-organized (SRBFN). The SRBFN focuses on the object (myocardium) in the image in an iterative process, until the contrast becomes clear (the fuzziness is close to zero).

As pointed out by Ghosh et al. [2] and according to our own experience on synthetic and real images, the index of fuzziness is better than the entropy measure for maintaining the compactness of the extracted objects. However, shapes of the objects are better preserved by the entropy measure. In Ref. [2], the authors explained this as follows: for the index of fuzziness the learning rate is lower than that of the entropy measure. Low learning rate smoothes out noises and creates compact regions, while entropy measure enables

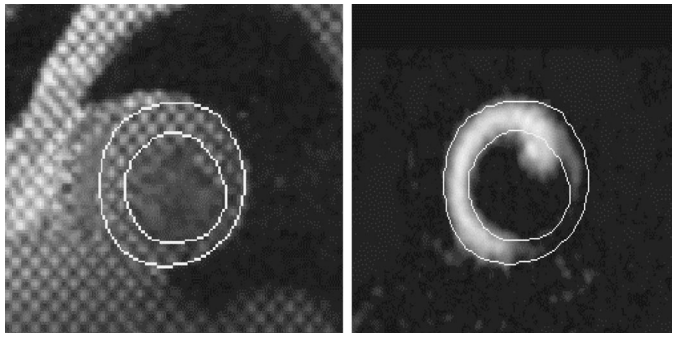

Fig. 11. Comparison between an image of the myocardium extracted from the PET data (right image) and an anatomical MR image of the heart (left image). The LV contours drawn on the MR image (on the left) have been superimposed on the PET image. One can notice the good correspondence in the thickness and shape of the LV.

the network to preserve object boundaries as learning rate is very high around the most ambiguous region ($o_j \approx 0.5$).

A sequential application of the two fuzziness measures made the SRBFN act in two phases. When an image is presented, the network will first detect a compact bright object (few iterations using the quadratic index of fuzziness) and then delineate accurately the borders of the object (few iterations using the entropy measure of fuzziness). For computing time efficiency reasons, the 3D-PET image is processed slice by slice. However, two orthogonal views of the image were considered and the intersection of the two extracted myocardium images constitutes the final result. Localization and estimation of the extent of the pathological region are much easier on the obtained 3D image. Besides the slice and polar-maps investigation, our visualization technique gives the physicians a more accurate estimate of the severity of the disease and the relationship between the defected coronary artery and the pathological territories. Furthermore, the automatic myocardium extraction allows automatic quantification of ^{18}FDG uptake. Indeed, the SRBFN extracts regions presenting reasonable to high ^{18}FDG-uptake, while excluding regions of severely decreased or absent metabolism.

8. Conclusion

The present paper describes an original and efficient approach to enable myocardium extraction in PET images using soft computing techniques. A RBFN, whose error is computed using fuzziness measures, has been successful in automatically extracting and delineating the myocardium. A sequential application of two fuzziness measures resulted in an RBFN performance comparable to that of a human expert (nuclear cardiologist). Indeed, the network first localizes bright and compact regions in the noisy (fuzzy) image and then focuses on the objects until they become clear. The output of the SRBFN allows a good 3D visualization of the LV by means of a ray tracing technique, showing an accurate delineation of the uptake defect. Furthermore, it is a valuable preprocessing step in the further quantification processes.

The presented network is currently integrated in a myocardial viability assessment package combining PET perfusion and tagging MRI images (Fig. 11) [17]. The extracted myocardium acts as a 3D region of interest in which blood flow analysis is concentrated, and contractile function parameters are fused with metabolism and perfusion to accurately assess myocardial viability.

References

[1] Garcia EV, Maddah KT, et al. Quantification of rotational Thallium-201 myocardial perfusion tomography. J. Nucl. Med. 1993:34–64.
[2] Gosh A, Pal NR, Pal SK. Self-organisation for object extraction using a multilayer neural network and fuzziness measures. IEEE Fuzzy Syst 1993;1:54–68.
[3] Dereks EPPA, Pastor Sanchez MS, Buydens LMC. Robustness analysis of radial basis function and multi-layered feed-forward neural network models. Chemomet Intelligent Lab Syst 1995;28:49–60.
[4] Tao KM. A closer look at the radial basis function networks. Proceeding of the Conference Record of the Twenty-Seventh Asilomar, Conference on Signals, Systems and Computers. Vol. 1, 1993. p. 401–05.
[5] Powell MJD. Radial basis function approximations to polynomials. Proceedings of the 12th Biennial Numerical Analysis Conference (Dundee), 1987. p. 223–41.
[6] Broomhead DS, Lowe D. Multivariable function interpolation and adaptative networks. Complex Syst 1988;12:321–55.
[7] Leonard JA, Kamer MA. Radial basis function networks for classifying process faults. IEEE Control Syst Mag 1991;11:31–38.
[8] Poggio T, Girosi F. Network for approximation and learning. Proc IEEE 1990;78:1481–97.
[9] Musavi MT, Ahmed W, Chan KH, Faris FB, Hummels DM. On the training of radial basis function classifiers. Neural Networks 1992;5(4):595–603.
[10] Hwang YS, Bang SY. An efficient method to construct a radial basis function neural network classifier. Neural Networks 1997;10(8):1495–503.
[11] Moody J, Darken C. Learning with localized receptive fields. Proceedings of the Connectionist Summer School (Carnergie Mellon).
[12] Kang HB, Walker EL. Characterising and controlling approximation in hierarchical perceptual grouping. Fuzzy Sets Syst 1994;65:187–223.
[13] Kosko B. Fuzzy entropy and condition. Inform Sci 1989;40:165–74.

[14] Pal NR, Pal SK. Higher order of fuzzy entropy and hybrid entropy of a set. Inform Sci 1992;61:211–31.
[15] Deluca A, Termini S. A definition of non probabilistic entropy in the setting of fuzzy set theory. Inform Control 1972;20:301–12.
[16] Kandel A. Fuzzy mathematical technique with applications. New York: Addison-Wesley, 1986.
[17] Behloul F, Janier M, Croisille P, Boudraa A, Unterreiner R, Mason JC, Revel D. Automatic assessment of myocardial viability based on PET-MRI data fusion. Proceedings of the 20th Annual International Conference of the IEEE Engineering in Medicine and Biology Society. Vol. 20, No. 1, 1998. p. 492–95.